



A versatile carbazole donor design strategy for blue emission switching from normal fluorescence to thermally activated delayed fluorescence

Rui Niu, Jiuyan Li^{*}, Di Liu^{**}, Ruizhi Dong, Wenkui Wei, Houru Tian, Chunlong Shi

State Key Laboratory of Fine Chemicals, School of Chemical Engineering, Dalian University of Technology, 2 Linggong Road, Dalian, 116024, China

ARTICLE INFO

Keywords:

Blue thermally activated delayed fluorescence (TADF)
Methyl-substituted carbazole
Steric hindrance
Organic light-emitting diodes (OLEDs)

ABSTRACT

The weak electron donating ability of carbazole is most suitable for constructing the donor-acceptor type blue emitters, but its low spatial requirements caused by the five-membered ring bridged structure is not favorable for spatial separation of frontier molecular orbitals. So many carbazole based compounds do not exhibit thermally activated delayed fluorescence (TADF). Herein, a more sterically demanding group was introduced at the 1-site of carbazole to form 1-methylcarbazole (1-MeCz), in order to construct a versatile donor for blue TADF materials. 1-MeCz was used as donor in combination with triazine and pyrimidine as acceptors to design novel compounds 1-MeCz-TRZ and 1-MeCz-Pm. It was observed that the presence of the methyl group at the 1-site of carbazole enhanced the twisted angles and reduced frontier molecular orbital overlapping, successfully switching the blue emission from the normal fluorescence of the methyl-free reference compounds (Cz-TRZ and Cz-Pm) to TADF of 1-MeCz-TRZ and 1-MeCz-Pm. The organic light-emitting diodes of 1-MeCz-TRZ and 1-MeCz-Pm exhibited blue emission at 450 and 458 nm with Commission Internationale de L'Eclairage (CIE) coordinates of (0.15, 0.11) and (0.17, 0.18), and external quantum efficiencies of 13.07% and 7.53%. This study provides a versatile, simple and practical design strategy with 1-MeCz to construct pure blue TADF emitters in combination with various acceptors.

1. Introduction

Nowadays, organic light-emitting diodes (OLEDs) have been highly attractive for solid state lighting and new-generation displays due to their wonderful performance such as flexibility, lightness and low-cost production, which can be dated back to the report by Tang and Van Slyke [1]. The singlet and triplet excitons, originating from electrically injected holes and electrons, combine in a ratio of 1:3 according to spin statistics [2,3]. For the OLEDs based on the normal fluorescent emitters, the internal quantum efficiencies (IQEs) are limited to 25% by dark triplet states. Most efforts have been devoted to achieving the ideal 100% IQEs and improving the external quantum efficiencies (EQEs) by activating the non-emissive triplet excitons. Hereafter, the emergence of transition-metal complex phosphors has extremely enhanced the device performance by harvesting the triplet excitons for light emission because of the spin-orbit coupling (SOC) effect [4,5]. However, the commercial applications of phosphorescent OLEDs (PhOLEDs) are difficult to move forward due to the utilization of noble metals. Fortunately, thermally activated delayed fluorescence (TADF) was reported first by Adachi's

group [6], as a novel pathway to achieve 100% IQE by using noble-metal free pure organic materials, only by means of the upconversion of triplet excitons to singlet ones through reverse intersystem crossing (RISC) process. A small energy gap between the lowest triplet (T_1) and (S_1) singlet excited states (ΔE_{ST}) is basically required for this mechanism, which can be achieved by appropriate molecular design. Since then, the OLEDs based on the pure organic TADF emitters manifest bright application prospects because they overcome the intrinsic shortcomings correlated with the traditional fluorescent and noble metal containing phosphorescent emitters [7–9].

Generally, TADF features can be obtained by the electron-donor- π -electron-acceptor (D- π -A) frameworks with intramolecular charge transfer (ICT) effect, with the prerequisite of narrow singlet-triplet energy splitting (ΔE_{ST}) [10]. In recent years, great progresses have been achieved in green and red TADF OLEDs with EQEs around 30% [11–14]. Pure blue TADF emitters for OLEDs, usually defined as y-axis value of Commission Internationale de l'Eclairage (CIE) coordinates (CIE_y) is above 0.10 with CIE_{x+y} below 0.30, are still the grand challenges at present, because a broad energy gap between the highest occupied

^{*} Corresponding author.

^{**} Corresponding author.

E-mail addresses: jiuyanli@dlut.edu.cn (J. Li), liudi@dlut.edu.cn (D. Liu).

<https://doi.org/10.1016/j.dyepig.2021.109581>

Received 18 April 2021; Received in revised form 18 June 2021; Accepted 18 June 2021

Available online 23 June 2021

0143-7208/© 2021 Elsevier Ltd. All rights reserved.

molecular orbital (HOMO) and the lowest unoccupied molecular orbital (LUMO) is essential for blue emission, composed by a donor with a deep HOMO and acceptor with a shallow LUMO. The previous reports demonstrated that the small ΔE_{ST} of TADF emitters could be realized by the rational spatial separation of HOMO and LUMO, which could reinforce the excitons upconversion process from T_1 to S_1 state via thermal activation. The electron-rich donor (e.g., bicarbazole derivatives) and the electron-withdrawing group (e.g., triazine) were directly linked to reduce the overlap between HOMO and LUMO [15]. Another design strategy is to increase torsion angle between donor and acceptor to achieve the effective separation of HOMO and LUMO. Recently, Yang reported CN-pyridine-based TADF emitters, with double-twist structure, which exhibited high EQEs of 25.8% in green region and 21.1% in yellow region [16]. A red TADF emitter with highly twisted D- π -A architecture has been developed by Chi's group with EQE of 7.13% at 635 nm with high photoluminescence quantum yield (PLQY) of 55% [17]. A sky blue TADF device was demonstrated a high EQE of 27.8% by Lee's group, where the selective twisting of the donor structure design strategy was applied [18].

Carbazole is weakly electron donating in comparison with other widely used donors including acridine, phenoxazine, and phenothiazine, and highly suitable for constructing blue emitters, since the charge transfer between donor and acceptor should be relatively weak if high excited state energy and thus blue emission is desired. At the same time, the planar structure of carbazole is beneficial to suppress the energy loss caused by the conformation change in the blue OLEDs [19–22]. However, the five-membered ring bridged structure and the resultant less steric hindrance of carbazole ring are not favorable for spatial separation of HOMO and LUMO. As a result, most of the carbazole based compounds do not exhibit TADF due to relatively large ΔE_{ST} values. To solve this problem, there are two common ways to design blue TADF molecules with the modified-carbazole: (a) different electron-donating groups are introduced to the carbazole ring in order to make the HOMO dispersed; (b) the bulky units, such as methyl or phenyl, are grafted on the carbazole at 1-site and/or 8-site, likewise on the phenylene bridge for D- π -A type molecules. It is an efficient strategy to tune the light-emitting mechanism with the small ΔE_{ST} by the delocalization of the HOMO and LUMO [23–26].

Herein, we investigate a general chemical modification of carbazole to switch the emission mechanism from normal fluorescence to TADF. A methyl (Me) group was introduced at the 1-site of carbazole (Cz) to generate the 1-methylcarbazole (1-MeCz), with the expectation that the strong steric hindrance of the relatively bulky methyl group will facilitate the rotation of carbazole ring to reduce the spatial repulsion between this methyl and the neighbouring group. 1-MeCz was used as versatile donor to design TADF emitters in combination with triazine and pyrimidine as acceptors. It is expected that the twist angle between carbazole donor and the bridge or acceptor will be increased and pure blue TADF can be achieved. Two novel compounds, namely 1-MeCz-TRZ and 1-MeCz-Pm, were designed and prepared in this way. The methyl-free compound, i.e. Cz-TRZ, was prepared as a reference for comparison. It was demonstrated that the normal fluorescence of methyl-free compounds (like Cz-TRZ) was successfully switched to blue TADF of 1-MeCz-TRZ and 1-MeCz-Pm. These compounds were used as doped emitters to fabricate blue OLEDs and exhibited acceptable performance. The 1-MeCz-TRZ device exhibited a maximum current efficiency of 12.16 cd A⁻¹ and an EQE of 13.07%, almost being twice of the Cz-TRZ based OLED, at the wavelength of 450 nm owing to the extra contribution of the delayed fluorescence proportion. The 1-MeCz-Pm based TADF-OLED also exhibited a current efficiency of 10.56 cd A⁻¹ and EQE of 7.53%. Obviously, this is a reasonable and effective strategy to reinforce the electroluminescence efficiency by methyl group introduction on the carbazole ring at a sterically demanding site, altering the emitting mechanism from the normal fluorescence to TADF.

2. Experimental section

2.1. General information

The ¹H NMR and ¹³C NMR spectra were measured in CDCl₃ using a 400 MHz and 126 MHz Bruker Avance II 400 and Bruker AVANCE III 500, respectively. The mass spectra were obtained on a HP1100LC/MSD MS spectrometer and matrix-assisted laser desorption/ionization (MALDI) micro mass spectrometry (MS) spectrometer. The fluorescence at room temperature and transient photoluminescence (PL) spectra were measured with an Edinburgh FLS1000 fluorescence spectrometer, while the low temperature fluorescence and phosphorescence spectra were measured on a Hitachi F-7000 fluorescence spectrometer at 77 K in 2-methyltetrahydrofuran. The ultraviolet–visible (UV–vis) absorption spectra measurements were performed on a Perkin-Elmer Lambda 650 spectrometer at room temperature. Thermogravimetric analyses (TGA) were carried out on a Perkin-Elmer thermogravimeter (Model TGA7) under a nitrogen (N₂) flow at a heating rate of 10 °C min⁻¹. The differential scanning calorimetry (DSC) studies were performed using a DSC 1/500 at a heating rate of 20 °C min⁻¹ under a nitrogen atmosphere. Cyclic voltammetry (CV) measurements were performed using an electrochemical workstation (CHI610E) at a scan rate of 100 mV s⁻¹ and a conventional three electrode configuration, which contains a glassy carbon working electrode, a Pt-wire counter electrode, and a saturated calomel electrode (SCE) reference electrode. All of the CV measurements were demonstrated under nitrogen-purged in dichloromethane (DCM) for the anodic scan and dimethylformamide (DMF) for the cathodic scan at room temperature, with 0.1 M tetrabutylammonium hexafluorophosphate as the supporting electrolyte. Absolute photoluminescence quantum yields (PLQYs) of the compounds were measured in doped films on a HAMAMATSU absolute PL quantum yield spectrometer (C11347).

2.2. OLED fabrication and measurements

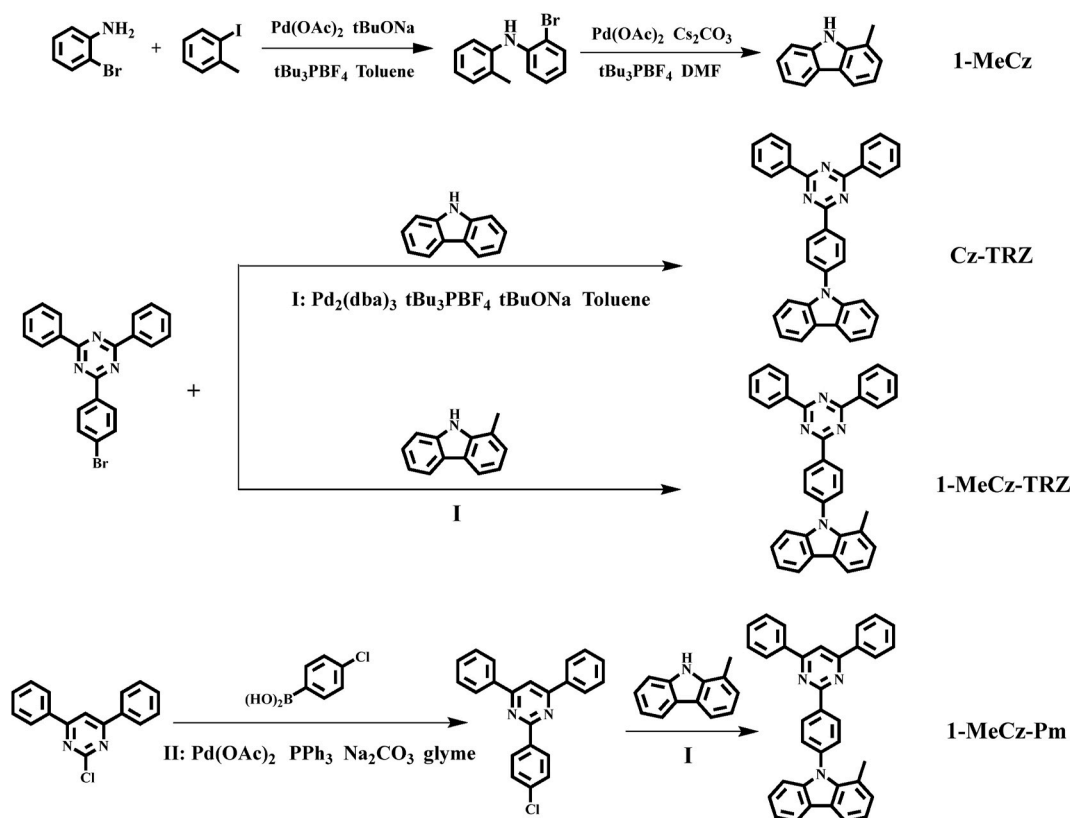
The pre-cleaned ITO glass substrates with a sheet resistance of 15 Ω m⁻² were first treated by UV-ozone for 30 min. Then a 40 nm thick PEDOT:PSS film was first deposited on the ITO glass substrate and baked at 120 °C for 30 min in air. Subsequently, the substrates were transferred into a vacuum chamber to deposit the organic layers with a base pressure of less than 10⁻⁶ Torr (1 Torr = 133.32 Pa). A thin layer of LiF (1 nm) and subsequently a thin layer of Al (200 nm) were vacuum deposited as the cathode, with the deposition rates of 0.1 Å s⁻¹ for LiF and 3–5 Å s⁻¹ for Al. The emitting area of each pixel was determined by the overlapping of the two electrodes as approximate 9 mm². The current density–voltage–brightness (*J-V-B*) curves of the devices were measured with Konica Minolta CS200 and a source-measure-unit (SMU) Keithley 2400 under ambient conditions at room temperature. The EL spectra and Commission Internationale de l'Eclairage (CIE) coordinates of the devices were measured with a PR705 photometer and a SMU Keithley 236 under ambient conditions at room temperature. The forward viewing external quantum efficiency was calculated using the current efficiency, EL spectra and human photopic sensitivity.

2.3. Compound synthesis

The intermediate 2-(4-bromophenyl)-4,6-diphenyl-1,3,5-triazine was synthesized according to the literature [27]. 1-Methylcarbazole (1-MeCz) was synthesized following the literature method [27], and the synthetic procedure is shown in Scheme 1.

2.3.1. Synthesis of 2-(4-chlorophenyl)-4,6-diphenyl-1,3-pyrimidine

A mixture of 4,6-diphenyl-1,3-pyrimidine (2.00 g, 7.50 mmol), 4-chlorophenylboronic acid (1.17 g, 7.50 mmol), anhydrous sodium carbonate (2.38 g, 22.50 mmol), palladium(II) acetate (17.00 mg, 0.07 mmol) and triphenylphosphine (59.00 mg, 0.22 mmol) were dissolved



Scheme 1. Chemical structures and synthetic routes of Cz-TRZ, 1-MeCz-TRZ, and 1-MeCz-Pm.

in ethylene glycol dimethyl ether (60 mL). Under nitrogen atmosphere, the mixture was stirred at 70 °C for 24 h. Upon cooling to room temperature, and reaction solvent was removed under reduced pressure. Then the crude product was purified by column chromatography on silica gel using dichloromethane/petroleum (1:20) as eluent to obtain a white powder. Yield: 78%. MALDI-TOF-MS (m/z): 343.0997 [M^+]. The comprehensive characterization data are identical to those in the literature report [28].

2.3.2. General procedure for syntheses of Cz-TRZ, 1-MeCz-TRZ, 1-MeCz-Pm

2-(4-bromophenyl)-4,6-diphenyl-1,3,5-triazine or 2-(4-chlorophenyl)-4,6-diphenyl-1,3-pyrimidine (5.00 mmol), Cz or 1-MeCz (5.50 mmol), tris(dibenzylideneacetone)dipalladium (0.25 mmol), tri-*tert*-butylphosphine tetrafluoroborate (0.75 mmol) and sodium *tert*-butoxide (10.00 mmol) were dissolved in dry toluene (150 mL) under N_2 atmosphere. After stirring at 120 °C for 24 h under N_2 atmosphere, the reaction solvent was removed by vacuum distillation, and the residue was purified by column chromatography on silica gel to afford the crude product. Repeated recrystallization from methanol/chloroform gave the pure products as white powders.

Cz-TRZ: Yield: 82%. ^1H NMR (400 MHz, CDCl_3) δ : 9.06 (d, $J = 8.3$ Hz, 1H), 8.89–8.82 (m, 2H), 8.21 (d, $J = 7.8$ Hz, 1H), 7.85 (d, $J = 8.2$ Hz, 1H), 7.64 (ddt, $J = 20.1, 13.6, 6.6$ Hz, 4H), 7.49 (t, $J = 7.6$ Hz, 1H), 7.37 (t, $J = 7.4$ Hz, 1H). ^{13}C NMR (126 MHz, CDCl_3) δ : 170.83 (s), 140.63 (s), 139.46 (s), 135.15 (s), 133.98 (s), 131.65 (s), 129.64 (s), 128.02 (s), 127.70 (s), 125.74 (s), 125.15 (s), 122.77 (s), 119.42 (s), 119.40 (s), 108.92 (s). TOF-EI-MS (m/z): calcd. for $\text{C}_{33}\text{H}_{22}\text{N}_4$ 474.1844, found 474.1847 [M^+]. Anal. calcd (%) for $\text{C}_{33}\text{H}_{22}\text{N}_4$, C, 83.52; H, 4.67; N, 11.81; Found: C, 83.51; H, 4.70; N, 11.83.

1-MeCz-TRZ: Yield: 75%. ^1H NMR (400 MHz, CDCl_3) δ : 9.54–8.51 (m, 6H), 8.18 (d, $J = 7.7$ Hz, 1H), 8.09 (dd, $J = 7.4, 1.7$ Hz, 1H), 7.73–7.55 (m, 7H), 7.46–7.38 (m, 1H), 7.37–7.18 (m, 5H), 2.17 (s,

3H); ^{13}C NMR (126 MHz, CDCl_3) δ : 171.88 (s), 170.95 (s), 143.61 (s), 142.57 (s), 139.59 (s), 136.11 (s), 136.05 (s), 132.72 (s), 129.88 (s), 129.56 (s), 129.06 (s), 128.94 (s), 128.74 (s), 126.00 (s), 124.36 (s), 123.50 (s), 121.42 (s), 120.24 (s), 120.16 (s), 120.10 (s), 118.24 (s), 110.01 (s), 20.06 (s). TOF-EI-MS (m/z): calcd. for $\text{C}_{34}\text{H}_{24}\text{N}_4$ 488.2001, found 488.2003 [M^+]. Anal. Calcd (%) for $\text{C}_{34}\text{H}_{24}\text{N}_4$, C, 83.58; H, 4.95; N, 11.47; Found: C, 83.54; H, 4.98; N, 11.45.

1-MeCz-Pm: Yield: 72%, M_p 202 °C. ^1H NMR (400 MHz, CDCl_3) δ : 8.96 (d, $J = 8.1$ Hz, 2H), 8.37 (dd, $J = 7.5, 2.1$ Hz, 4H), 8.18 (d, $J = 7.7$ Hz, 1H), 8.10 (d, $J = 17.3$ Hz, 2H), 7.74–7.56 (m, 8H), 7.46–7.37 (m, 1H), 7.32 (t, $J = 7.6$ Hz, 1H), 7.27–7.18 (m, 3H), 2.18 (s, 3H). ^{13}C NMR (126 MHz, CDCl_3) δ : 163.99 (s), 162.76 (s), 141.69 (s), 140.84 (s), 137.02 (s), 136.34 (s), 129.95 (s), 128.44 (s), 128.31 (s), 127.99 (s), 127.75 (s), 126.32 (s), 124.85 (s), 123.12 (s), 122.29 (s), 120.44 (s), 118.96 (s), 118.94 (s), 118.87 (s), 117.13 (s), 109.56 (s), 109.06 (s), 18.91 (s). MALDI-TOF-MS (m/z): calcd. for $\text{C}_{35}\text{H}_{25}\text{N}_3$ 487.2048, found 487.2065 [M^+]. Anal. Calcd (%) for $\text{C}_{35}\text{H}_{25}\text{N}_3$, C, 86.21; H, 5.17; N, 8.62. Found: C, 86.20; H, 5.19; N, 8.59.

3. Results and discussion

3.1. Synthesis and thermal properties

The chemical structures and synthetic procedures of these emitters are shown in Scheme 1. The intermediate 2-(4-bromophenyl)-4,6-diphenyl-1,3,5-triazine was synthesized according to previously reported methods [27]. 2-(4-chlorophenyl)-4,6-diphenyl-1,3-pyrimidine was synthesized via Suzuki coupling reaction. These three compounds were successfully prepared through Buchwald-Hartwig C–N coupling reaction of the corresponding acceptor intermediate with donor Cz or 1-MeCz in high yields. To meet the requirements for OLED application, all these emitters were thoroughly purified by silica gel column chromatography and repeated recrystallization in methanol/chloroform in

view of their good solubility in common organic solvents. ^1H NMR spectroscopy, mass spectrometry and elemental analysis were used to characterize the molecular structures.

The thermal properties of the emitters were investigated by thermogravimetric analysis (TGA) and differential scanning calorimetry (DSC). As shown by the TGA curves in Fig. S1(a), their thermal decomposition temperatures (T_d , corresponding to 5% weight loss) are detected at 386.53 and 334.13 °C for 1-MeCz-TRZ and 1-MeCz-Pm, respectively. During the second heating cycle in the DSC measurements (Fig. S1(b)), moderate glass transition temperatures (T_g) of 99 and 71 °C were observed for 1-MeCz-TRZ and 1-MeCz-Pm. At the same time, the melting points (T_m , i.e. M_p) of these two compounds were found at 231 and 202 °C for 1-MeCz-TRZ and 1-MeCz-Pm, respectively. As above,

the high T_d and moderate T_g values indicate good thermal stability of these compounds and stable OLEDs can be expected if they are used as emitters.

3.2. Theoretical calculation

The Gaussian 09 program suite was used to simulate the geometry configuration and frontier molecular orbitals of these molecules, based on density functional theory (DFT) calculations. The ground states (S_0) geometries and the lowest excited singlet and triplet states geometries (S_1 and T_1) were optimized at the B3LYP/6-31G(d) level and time-dependent DFT (TDDFT) at the same level, respectively. As depicted in Fig. 1, the HOMOs of all molecules locate mainly on the carbazole

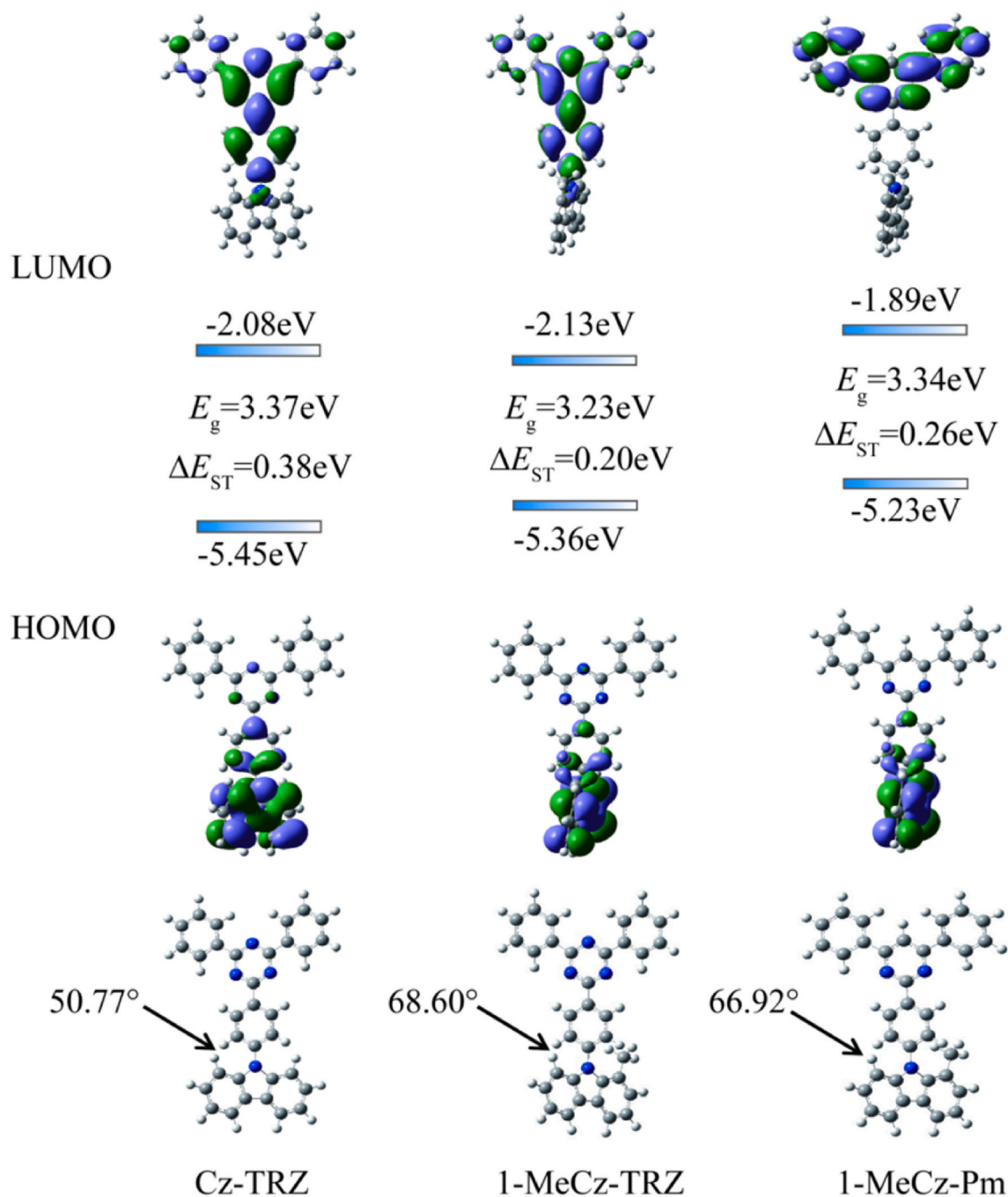


Fig. 1. Optimized geometries, HOMO and LUMO distributions in the optimized ground states, and the calculated energy levels for Cz-TRZ, 1-MeCz-TRZ, and 1-MeCz-Pm.

ring, with a little spreading onto the adjacent phenylene ring, and the LUMOs are distributed over the central electron withdrawing triazine or pyrimidine ring and the neighbouring phenyl or phenylene rings. The overlap degree of the HOMO and LUMO correlates with the steric molecular conformation and the torsion angles. As shown by the optimized geometries in Fig. 1 and 1-MeCz-TRZ and 1-MeCz-Pm have larger dihedral angles among three compounds because of the introduction of methyl group with tetrahedral structures at the 1-site of carbazole, which is in accordance with the molecular design principle of TADF types. For Cz-TRZ, the donor group has a dihedral angle of 50.77° with the phenylene ring. When methyl is introduced at the 1-site of carbazole, the dihedral angle in 1-MeCz-TRZ increased to 68.60° due to steric hindrance. As above, 1-MeCz-Pm has a similar dihedral angle between the carbazole ring and the phenylene bridge. As expected, with the introduction of the methyl at 1-site of carbazole, the degree of molecular distortion increased due to the steric hindrance effect, resulting in the effective separation of HOMO and LUMO. It is predicted that the large torsion will lead to small ΔE_{ST} and efficient RISC, ensuring the realization of TADF properties.

3.3. Electrochemical properties

The electrochemical properties of these molecules were investigated by means of cyclic voltammetry (CV) in oxygen-free dichloromethane (anodic scan) or dimethylformamide (cathodic scan) solutions at a scan rate of 100 mV s^{-1} . The cyclic voltammograms are shown in Fig. 2 and the related data are summarized in Table 1. On the basis of the oxidation curves, it is not difficult to figure out that all these compounds reveal an irreversible oxidation waves that should occur on the same carbazole moiety of each molecule. It can be discerned that the oxidation of two 1-MeCz containing compounds occurred at less positive potentials (E_{ox}^{onset}), i.e. Cz-TRZ (1.21 V), 1-MeCz-TRZ (1.15 V), and 1-MeCz-Pm (1.18 V). The HOMO energies were estimated according to the equation of $E_{HOMO} = -(E_{ox}^{onset} + 4.4)$, to be -5.61 , -5.55 , -5.58 eV for Cz-TRZ, 1-MeCz-TRZ, and 1-MeCz-Pm, respectively. It confirms that 1-methylcarbazole has greater electron-donating ability than the unsubstituted carbazole ring. The LUMO energies of these molecules were measured from the cathodic scan in a similar way. The onset potentials of the reduction waves (E_{red}^{onset}) for the three molecules Cz-TRZ, 1-MeCz-TRZ, and 1-MeCz-Pm are close to each other (-1.48 , -1.50 and -1.54 V). According to the equation $E_{LUMO} = -(E_{red}^{onset} + 4.4)$, the LUMO levels of these compounds were estimated to be -2.92 , -2.90 , and -2.86 eV ,

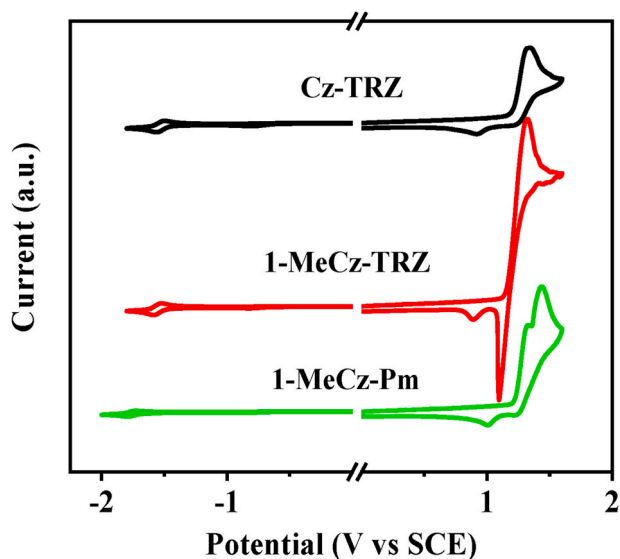


Fig. 2. Cyclic voltammograms measured in dilute DCM (anodic) and DMF (cathodic) solutions.

respectively. The electrochemical band gaps (E_g s) are determined as the potential difference between E_{red}^{onset} and E_{ox}^{onset} multiplied by the electron charge (e) to be 2.69, 2.65, 2.72 eV for Cz-TRZ, 1-MeCz-TRZ, and 1-MeCz-Pm, respectively. Evidently, the electrochemical results are consistent with the theoretical simulated ones.

3.4. Photophysical properties

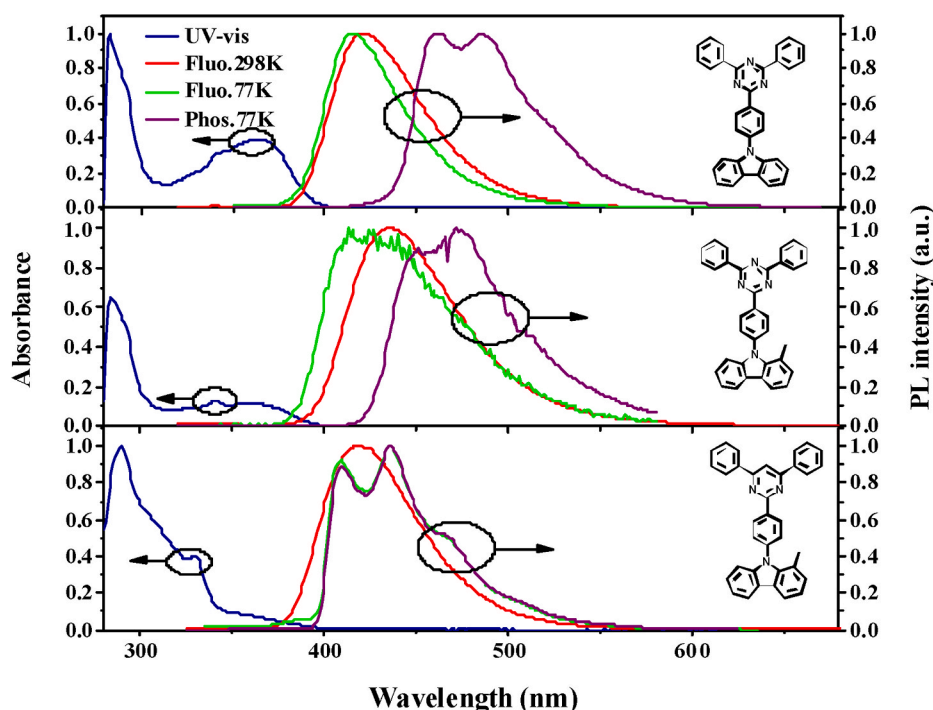
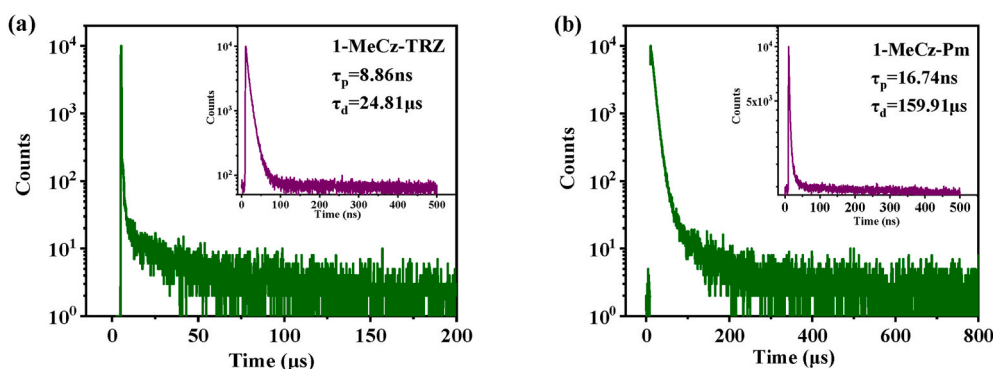
Photophysical properties of three emitters were analyzed using UV-vis and photoluminescence (PL) spectroscopies in dilute toluene solutions. As illustrated in Fig. 3, all compounds have a common strong absorption peaks at around 285 nm which belong to the $\pi-\pi^*$ transitions of the aromatic rings including the acceptor and donor units, and the weak absorption peaks at 320–340 nm could be assigned to the $n-\pi^*$ transitions of Cz or 1-MeCz. All compounds exhibited a broad and structureless absorption band in the wavelength range of 350–400 nm, which can be attributed to the intramolecular charge transfer (ICT) transition from the carbazole donor to the acceptor unit. All relevant data are summarized in Table 1. These compounds showed broad and featureless fluorescence spectra in dilute toluene solution upon optical excitation at the absorption maxima (Fig. 3), indicating the S_1 states of these compounds can be identified as 1CT states [27]. As well, the emission maximum of 1-MeCz-TRZ is redshifted by approximately 13 nm compared with Cz-TRZ (422 nm) because the electron donating ability is slightly enhanced by methyl group at 1-site of carbazole. The fluorescence peaks of 1-MeCz-Pm is centered at 420 nm in toluene solution. Furthermore, the ICT characteristic also can be confirmed by the gradual bathochromic shift of the fluorescence spectra with increasing the solvent polarity for each compound, as depicted in Fig. S2. Fig. 3 also illustrates the low-temperature (LT) fluorescence and phosphorescence spectra of Cz-TRZ, 1-MeCz-TRZ and 1-MeCz-Pm in a frozen 2-methyltetrahydrofuran (2-MeTHF) matrix at 77 K. Clearly, the phosphorescence spectra of Cz-TRZ, 1-MeCz-TRZ and 1-MeCz-Pm are well resolved and show characteristic vibrational structures, indicating that their T_1 states are 3LE states. The T_1 energies (E_T) of these compounds were determined from the short-wavelength onset of LT phosphorescence spectra to be 2.84 eV (Cz-TRZ), 2.76 eV (1-MeCz-TRZ), 2.95 eV (1-MeCz-Pm), respectively. Similarly, their S_1 energies (E_S) were calculated to be 3.20, 2.99 and 3.16 eV for Cz-TRZ, 1-MeCz-TRZ and 1-MeCz-Pm, respectively. Then ΔE_{ST} s were estimated to be 0.36, 0.23 and 0.21 eV for Cz-TRZ, 1-MeCz-TRZ and 1-MeCz-Pm, respectively. Delayed fluorescence may be possible for 1-MeCz-TRZ and 1-MeCz-Pm since the relatively small ΔE_{ST} is the prerequisite to realize efficient RISC process.

To better understand the light emitting mechanism of these compounds, the transient PL characteristics were analyzed for the doped films of these emitters in bis[2-(diphenylphosphino)phenyl]ether oxide (DPEPO) host at a doping concentration of 10 wt%. Transient PL decay curves of the doped films are shown in Fig. 4 and Fig. S3. Notably, prompt and delayed fluorescence components are clearly identified in doped films of 1-MeCz-TRZ and 1-MeCz-Pm. The lifetimes of the delayed components of 1-MeCz-TRZ and 1-MeCz-Pm doped films were determined as 24.81 and 159.91 μs , respectively. Conversely, the Cz-TRZ film did not exhibit any delayed fluorescence component, which should be because of its relatively large ΔE_{ST} . The reference compound of 1-MeCz-Pm, i.e. Cz-Pm, was ever reported in literature that it is only the traditional fluorescence compound [29]. Moreover, the temperature dependent transient PL decay was monitored from 100 to 300 K on the doped films to confirm the TADF nature for the two emitters. As depicted in Fig. S3, the intensity of the delayed fluorescence increased with increasing temperature gradually, especially in the short time range (e.g. in the first 100 μs range), indicating the long lifetime fluorescence components can be explicitly attributed to the TADF mechanism. Undesirably, 1-MeCz-TRZ and 1-MeCz-Pm both have a small proportion of delayed components, and their ratio of the prompt fluorescence (PF) to the delayed fluorescence (DF) is to be 5:1 and 20:1, respectively. The PL

Table 1

Basic parameters of the compounds.

| Compounds | $\lambda_{\text{abs}}/\lambda_{\text{em}}^{\text{a}}$ [nm] | HOMO/LUMO ^b [eV] | E_{g}^{c} [eV] | E_{T}^{d} [eV] | $\Delta E_{\text{ST}}^{\text{d}}$ [eV] | $\tau_{\text{PF}}/\tau_{\text{DF}}^{\text{e}}$ [ns/ μs] | Φ_{PL} [%] | $\Delta\lambda^{\text{f}}$ [nm] |
|------------|--|-----------------------------|--------------------------------|--------------------------------|--|---|------------------------|---------------------------------|
| Cz-TRZ | 280,325, 340,365/422 | -5.61/-2.94 | 2.67 | 2.84 | 0.36 | 7.42/- | 38.70 | 57 |
| 1-MeCz-TRZ | 285,326, 340,361/435 | -5.54/-2.97 | 2.57 | 2.76 | 0.23 | 8.86/24.81 | 51.30 | 74 |
| 1-MeCz-Pm | 289,330, 366/420 | -5.53/-2.81 | 2.72 | 2.95 | 0.21 | 16.74/159.91 | 42.10 | 54 |

^a Absorption and fluorescence peak wavelengths in toluene solutions.^b Determined from cyclic voltammetry measurements.^c $E_{\text{g}} = E_{\text{LUMO}} - E_{\text{HOMO}}$.^d Estimated from the short-wavelength onset of the fluorescence/phosphorescence spectra at 77 K in frozen 2-MeTHF, $\Delta E_{\text{ST}} = E_{\text{S}} - E_{\text{T}}$.^e Average lifetimes of prompt and delayed fluorescence in doped films.^f $\Delta\lambda$: Stokes shift, calculated as the wavelength difference of the charge transfer absorption and fluorescence bands in absorption and fluorescence spectra in toluene solution at room temperature.**Fig. 3.** UV-vis absorption and PL spectra of Cz-TRZ, 1-MeCz-TRZ and 1-MeCz-Pm in dilute toluene solutions at room temperature, and their LT fluorescence and phosphorescence spectra in frozen 2-MeTHF at 77 K.**Fig. 4.** Transient PL decay curves for the films of 1-MeCz-TRZ (a) and 1-MeCz-Pm (b) doped in DPEPO host (10 wt%) at 298 K.

spectra of 1-MeCz-TRZ and 1-MeCz-Pm in doped films (Fig. S4, Fig. S5) are slightly red-shifted to those in dilute toluene solutions. The fluorescence peaks of these films are centered at 449 and 456 nm, probably due to the high polarity of DPEPO [30]. In comparison with the normal fluorescence of the two reference compounds Cz-TRZ and Cz-Pm,

1-MeCz-TRZ and 1-MeCz-Pm were proved to have TADF character. It is evident that with the incorporation of methyl at the 1-site of carbazole, the blue emission was successfully switched from the normal fluorescence to TADF.

The absolute PL quantum yields (Φ_{PL}) of these emitters in doped

films (10 wt% in DPEPO) were measured as 38.70%, 51.30%, and 42.10% for Cz-TRZ, 1-MeCz-TRZ and 1-MeCz-Pm, respectively. According to the equations 1-8 listed in the supporting information, the exciton dynamics of the key transitions during the TADF process for TADF emitters were further analyzed and summarized in Table S1. As depicted, the radiative rate constants (k_r) of 1-MeCz-TRZ and 1-MeCz-Pm in doped films are higher than their intersystem crossing rate constants (k_{ISC}), indicating the singlet excitons that are thermally up-converted from T_1 state can generate delayed fluorescence before the remaining excitons go back to T_1 . The reverse intersystem crossing rate constants (k_{RISC}) of the TADF emitters were determined as $4.85 \times 10^4 \text{ S}^{-1}$ and $0.65 \times 10^4 \text{ S}^{-1}$, respectively, which are far below their intersystem crossing rates (k_{ISC}). The difficult RISC process from T_1 to S_1 lead to the relatively long delayed fluorescence lifetimes for these two TADF

emitters, even resulting in the nonradiative decay of T_1 state exacerbation and the poor device performance. Apparently, 1-MeCz-Pm has much lower k_{ISC} and k_{RISC} values than 1-MeCz-TRZ, which should be responsible for its longer delayed fluorescence lifetime in doped film.

3.5. Electroluminescent devices

To investigate the electroluminescence (EL) performance of the three emitters, the multilayered devices were fabricated with the structure of ITO/poly(3,4-ethylenedioxythiophene):polystyrene sulfonate (PEDOT:PSS, 40 nm)/1,1-bis[4-[N,N-di(p-tolyl)-amino]phenyl]cyclohexane (TAPC, 20 nm)/1,3-di(9H-carbazol-9-yl)benzene (mCP, 10 nm)/emitter: DPEPO (10 wt%, 20 nm)/DPEPO (10 nm)/1,3,5-tri[(3-pyridyl)-phen-3-yl]benzene (TmPyPB, 40 nm)/LiF(1 nm)/Al (200 nm) (devices D1 - D3

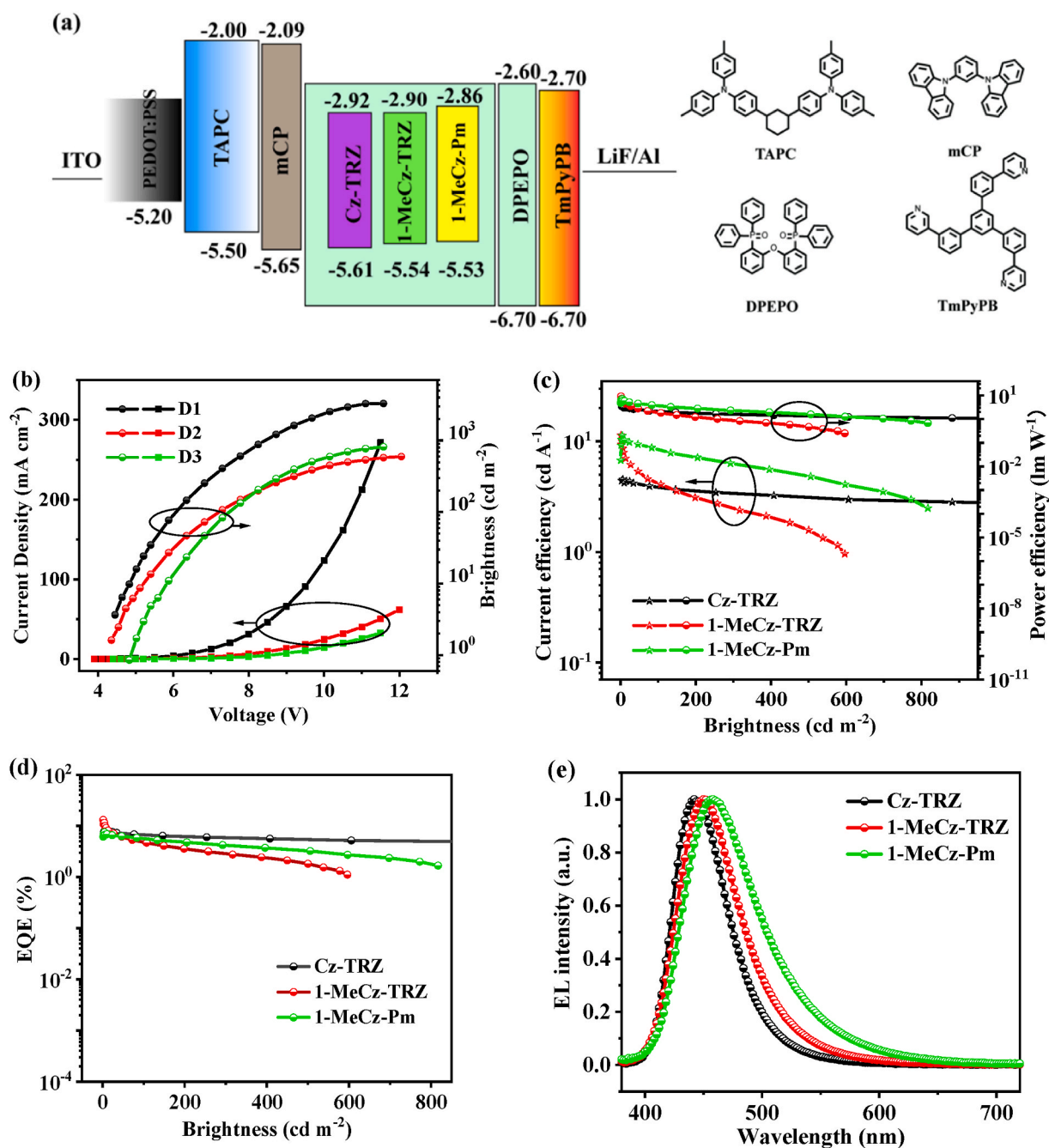


Fig. 5. (a) Device architecture and energy diagram for the vacuum deposited OLEDs and chemical structures of the relevant materials used for device fabrication, (b) J-V-B curves, (c, d) efficiency curves, and (e) EL spectra of blue OLEDs D1-D3.

for Cz-TRZ, 1-MeCz-TRZ and 1-MeCz-Pm, respectively). Therein, PEDOT:PSS played the role of hole injection layer due to its shallow HOMO level (-5.2 eV). TAPC and TmPyPB were used as the hole transporting layer (HTL) and electron transporting layer (ETL). mCP was selected as the electron blocking layer (EBL), and DPEPO was utilized as the host matrix and hole blocking layer (HBL) on the basis of their high E_T of mCP and DPEPO (mCP, $E_T = 2.9$ eV; DPEPO, $E_T = 3.1$ eV) [30,31]. The chemical structures and energy levels of these materials are shown in Fig. 5a, and all the key device performance parameters are summarized in Table 2. Three devices turned on (V_{on} , to deliver a luminance of 1 cd m^{-2}) at moderate voltages of 3.9–4.4 V. The J - V - B characteristics and efficiency curves of these devices are depicted in Fig. 5. As shown by the EL spectra, the TADF-OLEDs based on 1-MeCz-TRZ and 1-MeCz-Pm exhibited blue emission with peak wavelengths at 450 and 458 nm and CIE coordinates of (0.15, 0.11) and (0.17, 0.18) respectively.

As compared with Cz-TRZ based device D1, 1-MeCz-TRZ based device D2 revealed the superior performance with a maximum current efficiency (η_{CE}) of 12.16 cd A^{-1} , a power efficiency (η_{PE}) of 9.11 lm W^{-1} , and a maximum external quantum efficiency (η_{ext} , EQE) of 13.07%, which are all two times as high as reference device D1. This is reasonable because the TADF character of 1-MeCz-TRZ has additional contribution to the superior efficiency by means of harvesting the electrogenerated triplet excitons for light emission in OLEDs. For another TADF emitter 1-MeCz-Pm, device D3 showed the maximum η_{CE} of 10.56 cd A^{-1} and η_{PE} of 7.07 lm W^{-1} , corresponding to a maximum η_{ext} of 7.53%. It should be noted that the device efficiencies of both 1-MeCz-TRZ and 1-MeCz-Pm still have opportunity to be optimized, the relatively low proportion of DF in the overall emission for both two TADF emitters should be one of the main reasons responsible for their moderate performance. In addition, the slightly inferior efficiency of 1-MeCz-Pm device in comparison with 1-MeCz-TRZ may be because of the rather long DF lifetime of 1-MeCz-Pm (159.91 μs), which is definitely not favorable for an efficient radiation process. Therefore, it is still challenging to explore as many acceptors to construct blue TADF emitters to realized pure blue color and high efficiencies using 1-methylcarbazole as donor.

4. Conclusion

Overall, two twisted D- π -A TADF emitters, 1-MeCz-TRZ and 1-MeCz-Pm, based on methyl substituted carbazole donor were designed and synthesized. The optimized geometry of these compounds exhibited larger dihedral angle than methyl-free reference compound Cz-TRZ owing to the presence of methyl group at the 1-site of carbazole moiety. With the observation of the reduced ΔE_{ST} and the enhanced separation of HOMO and LUMO, the emitters based on 1-methylcarbazole (1-MeCz-TRZ and 1-MeCz-Pm) showed TADF properties compared to Cz-TRZ. The device fabricated using 1-MeCz-TRZ achieved a maximum current efficiency of 12.16 cd A^{-1} and EQE of 13.07% with pure blue color coordinates of (0.15, 0.11), which is higher than the maximum EQE of Cz-TRZ (7.61%). Meanwhile, the device containing 1-MeCz-Pm as doped TADF emitters exhibited a maximum EQE of 7.53% (10.56 cd A^{-1}) with color coordinates of (0.17, 0.18). The present molecular design strategy via molecular engineering of carbazole donor to switch the blue emission from normal fluorescence to TADF should be valid for large number of electron acceptors, for the purpose to develop various blue TADF materials with pure blue color and high performance.

Author contribution statement

Niu R, Li JY and Liu D designed the whole work; Niu R and Shi CL synthesized and characterized the properties of the compounds; Dong R and Wei WK fabricated and optimized the devices; Niu R wrote the paper with support from Tian HR. All authors contributed to the general discussion.

Table 2

EL performances of devices D1–3.

| Devices | V_{on} (V) | η_{CE}^a (cd A^{-1}) | η_{PE}^a (lm W^{-1}) | B_{max} (cd m^{-2}) | η_{ext}^b (%) | CIE (x, y) | λ_{EL} (nm) |
|---------|-----------------|---|---|-------------------------------------|-----------------------|-------------|------------------------|
| D1 | 4.0 | 4.86 | 3.46 | 3246 | 7.61, 6.63 | (0.15,0.07) | 442 |
| D2 | 3.9 | 12.16 | 9.11 | 596 | 13.07, 4.88 | (0.15,0.11) | 450 |
| D3 | 4.4 | 10.56 | 7.07 | 817 | 7.53, 5.69 | (0.17,0.18) | 458 |

^a The efficiencies are maximum values.

^b Order of measured values: maximum, then at 100 cd m^{-2} .

Declaration of competing interest

The authors declare that they have no known competing financial interests or personal relationships that could have appeared to influence the work reported in this paper.

Acknowledgments

We thank the National Natural Science Foundation of China (22078051 and U1801258), the Fundamental Research Funds for the Central Universities (DUT19ZD217, DUT19TD28), the Open Funds of State Key Laboratory of Fine Chemicals (KF1901), and the Open Fund of the State Key Laboratory of Luminescent Materials and Devices (South China University of Technology, 2021-skllmd-03) for financial support of this work.

Appendix A. Supplementary data

Supplementary data to this article can be found online at <https://doi.org/10.1016/j.dyepig.2021.109581>.

References

- [1] Tang CW, VanSlyk SA. Organic electroluminescent diodes. *Appl Phys Lett* 1987;51:913–5.
- [2] Friend RH, Gymer RW, Holmes AB, et al. Electroluminescence in conjugated polymers. *Nature* 1999;397:121–8.
- [3] Uoyama H, Goushi K, Shizu K, Nakamura H, Adachi C. Highly efficient organic light-emitting diodes from delayed fluorescence. *Nature* 2012;492:234–8.
- [4] Skaisgiris R, Serevičius T, Kazlauskas K, et al. Origin of dual emission in σ -bridged donor - acceptor TADF compounds. *J Mater Chem C* 2019;7:12601–9.
- [5] Baldo MA, Brien DFO, You Y, et al. Highly efficient phosphorescent emission from organic electroluminescent devices. *Nature* 1998;395:151–4.
- [6] Uoyama H, Goushi K, Shizu K, et al. Highly efficient organic light-emitting diodes from delayed fluorescence. *Nature* 2012;492:234–8.
- [7] Ma YG, Zhang HY, Shen J, Che CM. Electroluminescence from triplet metal-ligand charge-transfer excited state of transition metal complexes. *Synth. Met.* 1998;94:245–8.
- [8] Endo A, Sato K, Yoshimura K, Kai T, Kawada A, et al. Efficient up-conversion of triplet excitons into a singlet state and its application for organic light emitting diodes. *Appl Phys Lett* 2011;98:083302.
- [9] Cai XY, Su SJ. Marching toward highly efficient, pure-blue, and stable thermally activated delayed fluorescent organic light-emitting diodes. *Adv Funct Mater* 2018;28:1802558.
- [10] Chen XL, Jia JH, Yu R, Liao JZ, et al. Combining charge-transfer pathways to achieve unique thermally activated delayed fluorescence emitters for high-performance solution-processed, non-doped blue OLEDs. *Angew Chem Int Ed* 2017;56:15006–9.
- [11] Wu TL, Huang MJ, Lin CC, Huang PY, et al. Diboron compound-based organic light-emitting diodes with high efficiency and reduced efficiency roll-off. *Nat Photonics* 2018;12:235–40.
- [12] Zhang YL, Ran Q, Wang Q, Liu Y, et al. High-efficiency red organic light-emitting diodes with external quantum efficiency close to 30% based on a novel thermally activated delayed fluorescence emitter. *Adv Mater* 2019;31:1902368.
- [13] Wong MY, Colman EZ. Purely organic thermally activated delayed fluorescence materials for organic light-emitting diodes. *Adv Mater* 2017;29:1605444.
- [14] Godumala M, Choi S, Choa MJ, Cho DH. Thermally activated delayed fluorescence blue dopants and hosts: from the design strategy to organic light-emitting diode applications. *J Mater Chem C* 2016;4:11355–81.

- [15] Lee SY, Yasuda T, Nomura H, Adachi C. High-efficiency organic light-emitting diodes utilizing thermally activated delayed fluorescence from triazine-based donor-acceptor hybrid molecules. *Appl Phys Lett* 2012;101:93306.
- [16] Li JF, Chen WC, Liu H, et al. Double-twist pyridine-carbonitrile derivatives yielding excellent thermally activated delayed fluorescence emitters for high-performance OLEDs. *J Mater Chem C* 2020;8:602–6.
- [17] Wu Y, Chen X, Mu Y, Yang Z, Mao Z, et al. Two thermally stable and AIE active 1,8-naphthalimide derivatives with red efficient thermally activated delayed fluorescence. *Dyes Pigments* 2019;169:81–8.
- [18] Lee HL, Lee KH, Lee JY. Transformation from nonthermally activated delayed fluorescence molecules to thermally activated delayed fluorescence molecules. *Adv Optical Mater* 2020;8:2001025.
- [19] Zhang D, Cai M, Zhang Y, Zhang D, Duan L. Sterically shielded blue thermally activated delayed fluorescence emitters with improved efficiency and stability. *Mater Horiz* 2016;3:145–51.
- [20] Kim M, Jeon SK, Hwang SH, Lee JY. Stable blue thermally activated delayed fluorescent organic light-emitting diodes with three times longer lifetime than phosphorescent organic light-emitting diodes. *Adv Mater* 2015;27:2515–20.
- [21] Cui LS, Deng YL, Tsang DPK, Jiang ZQ, et al. Controlling synergistic oxidation processes for efficient and stable blue thermally activated delayed fluorescence devices. *Adv Mater* 2016;28:7620–5.
- [22] Wang K, Zheng CJ, Liu W, Liang K, Shi Y-Z, et al. Avoiding energy loss on TADF emitters: controlling the dual conformations of D-A structure molecules based on the pseudoplanar segments. *Adv Mater* 2017;29:1701476.
- [23] Kaji H, Suzuki H, Fukushima T, Shizu K, Suzuki K, et al. Purely organic electroluminescent material realizing 100% conversion from electricity to light. *Nat Commun* 2015;6:8476.
- [24] Li X, Li JY, Liu D, Dong RZ. Donor design strategy for triazine-carbazole blue thermally activated delayed fluorescence materials. *New J Chem* 2020;44:9743–53.
- [25] Li HT, Li JY, Liu D, Mei YQ. Mechanism evolution from normal fluorescence to thermally activated delayed fluorescence and color tuning over visible light range: effect of intramolecular charge transfer strength. *Dyes Pigments* 2020;183:108732.
- [26] Hirata S, Sakai Y, Masui K, Tanaka H, Lee SY, et al. Highly efficient blue electroluminescence based on thermally activated delayed fluorescence. *Nat Mater* 2015;14:330–6.
- [27] Cui LS, Nomura H, Geng Y, Kim JU, Nakanotani H, Adachi C. Controlling singlet-triplet energy splitting for deep-blue thermally activated delayed fluorescence emitters. *Angew Chem Int Ed* 2017;56:1571–5.
- [28] Mondal R, Sinha S, Das S, Chakraborty G, Paul ND. Iron catalyzed synthesis of pyrimidines under air. *Adv Synth Catal* 2020;362:594–600.
- [29] Iwasaki Y, Fukagawa H, Shimizu T. Effect of host moieties on the phosphorescent spectrum of green platinum complex. *Molecules* 2019;24:454.
- [30] Zhang QS, Komino T, Huang S, Matsunami S, Goushi K, Adachi C. Triplet exciton confinement in green organic light-emitting diodes containing luminescent charge-transfer Cu(I) complexes. *Adv Funct Mater* 2012;22:2327–36.
- [31] Yeh SJ, Wu M-F, Chen CT, Song Y-H, et al. New dopant and host materials for blue-light-emitting phosphorescent organic electroluminescent devices. *Adv Mater* 2005;17:285–9.